



University of HUDDERSFIELD

University of Huddersfield Repository

Tang, Dawei, Gao, Feng and Jiang, Xiangqian

On-line surface inspection using cylindrical lens-based spectral domain low-coherence interferometry

Original Citation

Tang, Dawei, Gao, Feng and Jiang, Xiangqian (2014) On-line surface inspection using cylindrical lens-based spectral domain low-coherence interferometry. *Applied Optics*, 53 (24). pp. 5510-5516. ISSN 1559-128X

This version is available at <http://eprints.hud.ac.uk/id/eprint/22242/>

The University Repository is a digital collection of the research output of the University, available on Open Access. Copyright and Moral Rights for the items on this site are retained by the individual author and/or other copyright owners. Users may access full items free of charge; copies of full text items generally can be reproduced, displayed or performed and given to third parties in any format or medium for personal research or study, educational or not-for-profit purposes without prior permission or charge, provided:

- The authors, title and full bibliographic details is credited in any copy;
- A hyperlink and/or URL is included for the original metadata page; and
- The content is not changed in any way.

For more information, including our policy and submission procedure, please contact the Repository Team at: E.mailbox@hud.ac.uk.

<http://eprints.hud.ac.uk/>

On-line surface inspection using cylindrical lens-based spectral domain low-coherence interferometry

Dawei Tang, Feng Gao,* and X. Jiang

Centre for Precision Technologies, University of Huddersfield, Huddersfield HD1 3DH, UK

*Corresponding author: F.Gao@hud.ac.uk

Received 7 May 2014; revised 17 July 2014; accepted 18 July 2014;
posted 21 July 2014 (Doc. ID 211612); published 18 August 2014

We present a spectral domain low-coherence interferometry (SD-LCI) method that is effective for applications in on-line surface inspection because it can obtain a surface profile in a single shot. It has an advantage over existing spectral interferometry techniques by using cylindrical lenses as the objective lenses in a Michelson interferometric configuration to enable the measurement of long profiles. Combined with a modern high-speed CCD camera, general-purpose graphics processing unit, and multicore processors computing technology, fast measurement can be achieved. By translating the tested sample during the measurement procedure, real-time surface inspection was implemented, which is proved by the large-scale 3D surface measurement in this paper. ZEMAX software is used to simulate the SD-LCI system and analyze the alignment errors. Two step height surfaces were measured, and the captured interferograms were analyzed using a fast Fourier transform algorithm. Both 2D profile results and 3D surface maps closely align with the calibrated specifications given by the manufacturer. © 2014 Optical Society of America

OCIS codes: (070.4790) Spectrum analysis; (120.3180) Interferometry; (120.3940) Metrology; (120.4630) Optical inspection.

<http://dx.doi.org/10.1364/AO.53.005510>

1. Introduction

Surfaces act as interfaces that have a direct influence on the functional behavior of a product [1]. Rapidly developing industries such as MEMS, micro fluidics, photovoltaic thin films, Si wafers, and hard disks critically rely on micro/nano-scale and ultraprecision structured surfaces [2]. In the industries making high-volume as well as large-area foil products and flexible electronics, the deposition and patterning of multilayer thin films on large-area substrates is often involved in manufacturing processes. For this type of product, the films must be uniform and largely perfect across most of the area of the foil. Evaluation of these surfaces by an expensive

trial-and-error approach is unadvisable due to the high scrap rate. To achieve a high product yield, the key challenge is therefore to inspect the foil surface at production speed as well as have sufficient resolution to detect the defects resulting from the coating and patterning processes. After effective inspection, further processes such as the local repair technique can be applied to remove defects.

Optical interferometry is a noncontact measurement technique widely used for precise surface metrology. It has potential application in on-line measurement with fine vertical and lateral resolution. Nevertheless, monochromatic interferometry is limited to the measurement of relatively smooth surfaces due to the well-known phase ambiguity problem. White light interferometry (WLI), using broadband illumination such as superluminescent diodes and halogen lamps, has been used for

1559-128X/14/245510-07\$15.00/0
© 2014 Optical Society of America

determining the absolute distance between the testing surface and the reference surface without the 2π phase ambiguity problem [3–5]. In general, it can be classified into three types, namely vertical scanning interferometry (VSI) [6], wavelength scanning interferometry (WSI) [7], and spectral domain low-coherence interferometry (SD-LCI), also called spectrally resolved white light interferometry (SRWLI) in other literature [8].

VSI enables the absolute measurement of the optical path difference (OPD) by determining the peak position from the interferogram. It has the disadvantage of utilizing mechanical scanning in the depth direction to localize the fringes in the vicinity of zero OPD, which is time consuming and permits measurement only for stationary objects [9]. As for WSI and SD-LCI, they belong to spectral interferometry, which takes advantage of spectral interference fringes for a wide range of wavelengths without any mechanical scanning [8,10,11]. The mechanical movement is replaced by the spectral decomposition of the output of the spectrometer [12]. As for the fast on-line surface inspection, the WSI is limited to some extent because many frames need to be captured for each measured area, which means in this capture time the tested sample should be kept still, and the compensation of environmental noise needs to be taken into consideration to achieve high measurement accuracy [13].

The SD-LCI system performing on-line measurement in a single shot is preferred over WSI. There has been considerable interest in SD-LCI since it was first proposed by Schwider and Zhou [14], for the purpose of retaining the unambiguous measurement advantage while eliminating mechanical scanning. Furthermore, the development of computers and spectrometers has allowed for SD-LCI for many applications, such as measuring the differential index of refraction, the distance and displacement, the thickness of the thin film, and the profile [15,16]. However, in all these existing SD-LCI techniques, spherical lenses such as micro-objectives were utilized to establish the interferometric objective, which gives only a small measuring range.

In this paper, a new spectral domain low-coherence interferometric technique aimed at long profile on-line surface measurement is presented. Instead of the microscope objectives used in current spectral interferometers, cylindrical lenses are employed to enable the measurement of long profiles. The adjustable profile length in our experimental setup, determined by the NA of the illuminating system and the aperture of cylindrical lenses, is up to 10 mm. To simulate real-time surface inspection, large-scale 3D surface measurement was carried out by translating the tested sample during the measurement procedure. The measurement results show that cylindrical lens-based SD-LCI has the potential to be used for on-line surface inspection with long profiles, such as surface metrology for roll-to-roll film processing, micro/nano-structured surfaces, lithographic etching

processing, doping, CVD/PVD coating, lapping, and CMP processing.

2. Methodology

A. Dispersion Principle

Different from WSI using an acoustic-optic tunable filter (AOTF) for wavelength scanning, SD-LCI employs a grating or dispersive prism to separate a series of constituent monochromatic interferograms that encode the phase as a function of wavenumber along the horizontal axis of the CCD camera (chromaticity axis) [17]. For a diffraction grating with space d , if a plane wave is incident with an angle θ_i , the diffraction angle is θ_m at the order m ; then for a beam with wavelength λ , the following equation should be satisfied:

$$m\lambda = d(\sin \theta_i + \sin \theta_m). \quad (1)$$

By selecting a proper grating spacing, the distance and the angle between the grating and CCD camera, it is expected that a desired spectral band of light can be captured with respect to the CCD pixels.

B. Wavelength Calibration

The optimum position of the CCD and angle of the grating were set to acquire the spectral waveband with relatively high intensity. In order to get the specific wavelengths with respect to the CCD pixels, experimental calibration should be carried out. Generally speaking, the chromaticity axis of the CCD camera is calibrated with a cadmium spectral lamp, which has four spectral lines. The wavelengths of the remaining pixels are then given using Hartmann's formula. In our experiment, a white light laser source (WhiteLase micro) in conjunction with an AOTF is used for this purpose. WhiteLase micro is an ultracompact supercontinuum source based on a mode-locked fiber laser, which possesses output power of more than 200 mW and covers a broad waveband of at least 450 to 2000 nm. By placing an AOTF behind the white light laser, a specific wavelength with high accuracy can be selected. The selected wavelength is determined by

$$\lambda = \Delta n \alpha v_a / f_a, \quad (2)$$

where Δn is the birefringence of the crystal used as the diffractive material, α is a parameter depending on the AOTF, and v_a , and f_a are the propagation velocity and frequency of the acoustic wave, respectively.

20 sampling points along the chromaticity axis of the CCD were calibrated. Two curves, showing the calibrated wavelength with respect to each pixel, were respectively obtained by using higher-order polynomial fitting of experimental data and Hartmann's formula defined as [18]

$$\lambda = \lambda_0 + \frac{C}{d_0 - d}, \quad (3)$$

where λ_0 , C , and d_0 are constants. Using three pairs of (λ, d) (three sample points) we can obtain the values of three unknown constants, and then the relation between wavelength λ and the pixel number d can be acquired by substituting the values of these constants in Eq. (3).

This calibration is verified by agreement of the fitting curve using the actual experimental data and the curve by Hartmann's formula, as depicted in Fig. 1.

C. Phase Calculation

The spectral intensity $I(x, y; \sigma)$ recorded at the output of the interferometer can be expressed as

$$I(x, y; \sigma) = a(x, y; \sigma) + b(x, y; \sigma) \cos[\varphi(x, y; \sigma)], \quad (4)$$

where (x, y) are the spatial coordinates of the interferogram, $a(x, y; \sigma)$ and $b(x, y; \sigma)$ are the background intensity and fringe visibility, respectively, and the phase $\varphi(x, y; \sigma)$ is linearly related to the wavenumber, which is defined by the formula

$$\varphi(x, y; \sigma) = \frac{4\pi}{\lambda} \times h(x, y) + \varphi_0 = 4\pi\sigma h(x, y) + \varphi_0, \quad (5)$$

where $h(x, y)$ represents the surface elevation, φ_0 is the initial phase, and σ is the wavenumber.

There are many algorithms to analyze the interferograms with white light illumination, such as Fourier transform [19], convolution [20], temporal phase shifting [17], Hilbert transform [21], and wavelet transform [22]. It turns out that the temporal phase shifting technique could give the most accurate results, which at the same time can determine the sign of measured height. However, the phase shifting method has a limitation in measuring a surface profile in motion. In this paper, we use a fast Fourier transform (FFT)-based algorithm to determine the phase from the interferogram and finally to calculate the point elevation from the slope of the phase distribution.

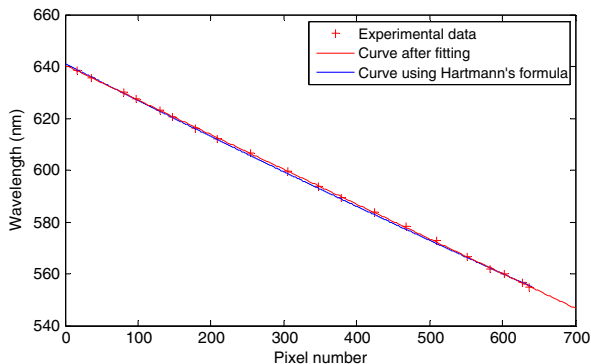


Fig. 1. Wavelength calibration of the CCD.

The interferogram recorded by the CCD camera contains background intensity variation, which results from the spectral distribution of the halogen lamp. By blocking the measurement arm of the interferometer, the background frame is captured without interference effect. Figure 2 generally shows the original signal and the signal after removing the background.

The original channeled spectrum is registered by the CCD with respect to the pixel number d (or wavelength λ). The phase variation is linear with wavenumber; therefore, the original sinusoidal signals with respect to the wavelength λ should be changed to the wavenumber ($\sigma = 1/\lambda$) related curve. Afterward, the phase along the chromaticity axis with respect to the wavenumber σ is extracted using the FFT method, which gives the wanted phase term by filtering out the direct current term and conjugate term of the phase from the power spectral density of the fringe pattern. FFT is used to extract the phase because it is fast, accurate, and insensitive to intensity noise [13]. Equation (4) can be rewritten as

$$I(x, y; \sigma) = a(x, y; \sigma) + c(x, y; \sigma) + c^*(x, y; \sigma) \quad (6)$$

with

$$c(x, y; \sigma) = \frac{1}{2} b(x, y; \sigma) \exp[i\varphi(x, y; \sigma)], \quad (7)$$

where $*$ denotes a complex conjugate. After Fourier transform, Eq. (6) can be written as

$$\tilde{I}(x, y; f) = A(x, y; f) + C(x, y; f) + C^*(x, y; f), \quad (8)$$

where the capital letters denote the Fourier spectra and f is the spatial frequency. After filtration of the unwanted background variation in the frequency domain, the desired term $C(x, y; f)$ is selected to compute the inverse fast Fourier transform (IFFT).

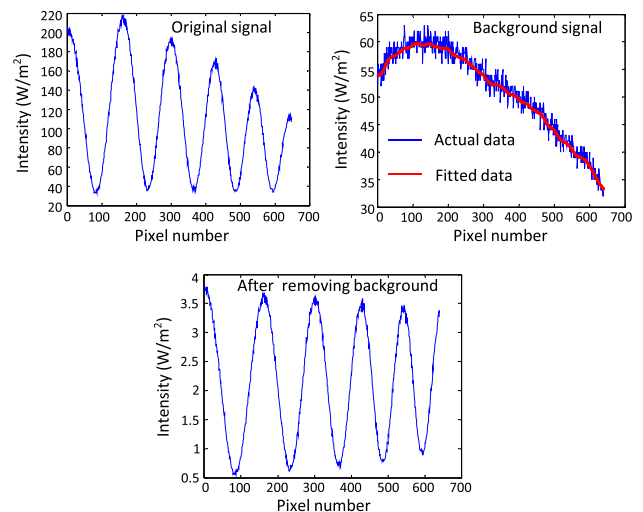


Fig. 2. Removing the background before phase is retrieved.

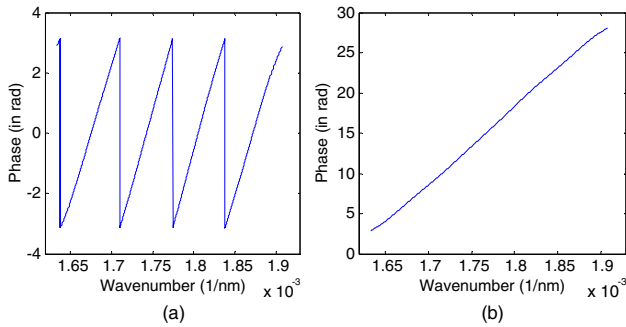


Fig. 3. Phase profile of the white light interferogram: (a) wrapped phase and (b) unwrapped phase.

Taking the natural logarithm of the IFFT $[C(x, y; f)]$, finally the phase $\varphi(x, y; \sigma)$ of each point is extracted as the imaginary part of Eq. (9):

$$\begin{aligned} & \log \left\{ \frac{1}{2} b(x, y; \sigma) \exp[i\varphi(x, y; \sigma)] \right\} \\ &= \log \left[\frac{1}{2} b(x, y; \sigma) \right] + i\varphi(x, y; \sigma). \end{aligned} \quad (9)$$

Additionally, the phase unwrapping process, illustrated in detail by Takeda *et al.* in 1982 [19], is performed to the discontinuities phase distribution. By comparing each point in the discontinuities phase distribution to the one preceding it, a 2π value should be added wherever there is a 2π phase jump. With the addition of the offset phase to the discontinuous

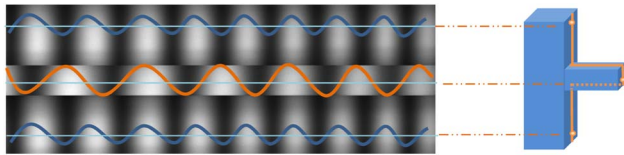


Fig. 4. Fringe pattern of step height obtained by SD-LCI.

determined phase, the corrected continuous phase is obtained as shown in Fig. 3. Finally, the point elevation is calculated from the slope of the phase distribution, which can be expressed as [23]

$$h = \frac{\Delta\varphi}{4\pi(1/\lambda_m - 1/\lambda_n)}, \quad (10)$$

where λ_m , and λ_n are the wavelengths corresponding to the phase difference $\Delta\varphi$.

Figure 4 shows the fringe pattern of the step object obtained by SD-LCI. The height map of a 1D profile on the tested surface can then be acquired after analysis of a series of row signals.

3. Experimental Setup

A. Schematic Diagram of Proposed System

The schematic diagram of the proposed cylindrical lens-based SD-LCI is shown in Fig. 5. The whole system mainly comprises four parts, namely a white light source, an interferometric objective, a spectrometer, and a data processing unit. The white light beam is coupled into an optical fiber patch cable and then collimated by a collimator. The tested surface is observed through a cylindrical lens-based Michelson interferometric objective ($f' = 75$ m). Interference occurs when two beams of light reflected from the reference arm and measurement arm are brought together. An iris diaphragm in conjunction with a compressor objective can adjust the profile length to meet different requirements of the system's spatial resolution. The interferogram is imaged on the slit to block the light that is redundant for measurement. Only a narrow line of light that represents an interference signal of a surface profile passes through the slit. After this slit light passes the spectrometer, channeled spectrum is observed through the CCD camera (ICL-B0620 from Imperx). By selecting a proper

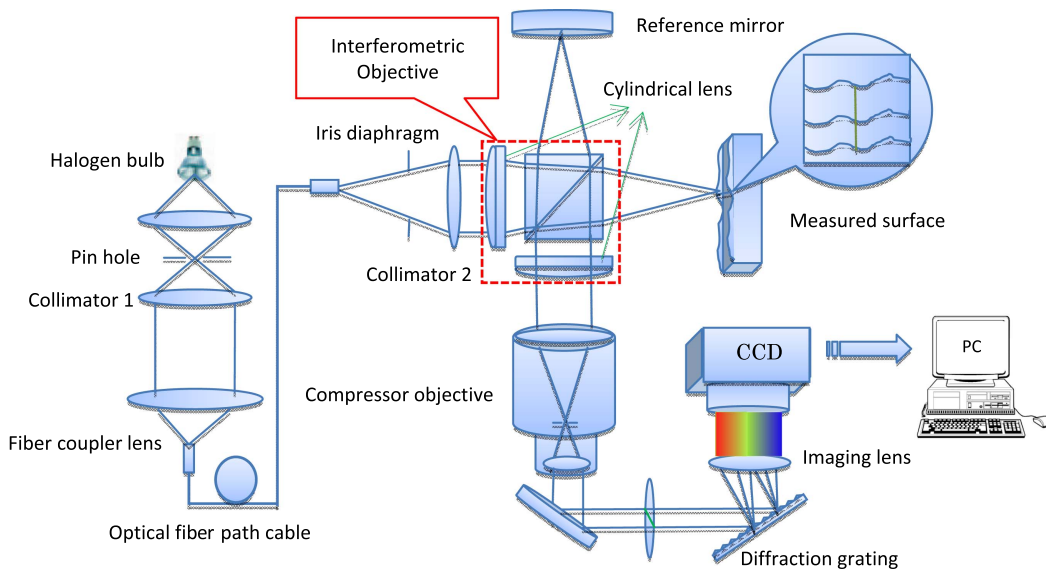


Fig. 5. Schematic diagram of the optical setup.

grating spacing and adjusting the position of the CCD camera, a desired waveband can be captured with overall consideration of the spectral curve of the light source. When the spectral interferograms were analyzed by the computational unit with appropriate algorithms at the same time, on-line inspection of the sample surface could be achieved.

If the SD-LCI is well aligned, zero fringes can be seen through the CCD camera due to the sample plane coincidence with the virtual reference plane. However, in order to determine the height direction (step or groove), the tested sample is expected to move along the optical axis until several fringes appear in the measuring field. It is at this position that the frame will be captured and analyzed by the data processing unit. The frame rate of the CCD camera used is higher than 200 fps. To simulate on-line inspection of the sample surface, the camera was set at continuous mode and the sample was translated at a speed of 0.5 mm/s during the measurement procedure; 1000 frames can be then obtained in 5 s, which means 1000 profiles are sampled on the tested surface across the width of 2.5 mm within this time.

B. Simulation by Zemax Software

The SD-LCI system was modeled as well using Zemax software in the sequential mode. Interferograms were simulated to better understand the influence from the alignment errors, which benefits the building of the experimental setup in terms of good alignment. With the aid of the multiconfiguration function in software, the 3D layout of the cylindrical lens-based spectral interferometry is shown in Fig. 6.

There are mainly two kinds of misalignments, namely tilts and offsets of the optical components. Tilt errors are of particular interest in our simulation, as shown in Fig. 7. Figure 8(a) indicates that tilts of the cylindrical lens only lead to deformation of the line focusing beam on the tested surface. More specifically, tilts about the X axis and Y axis make the

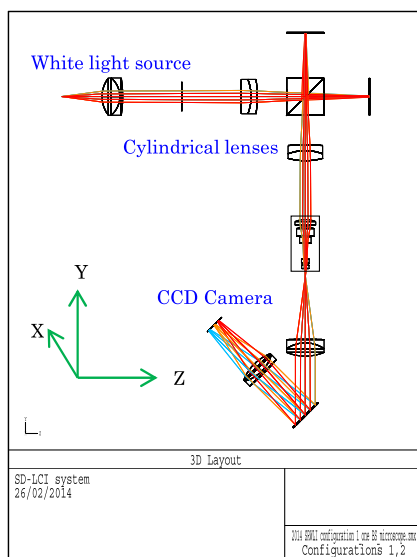


Fig. 6. 3D layout of SD-LCI by Zemax.

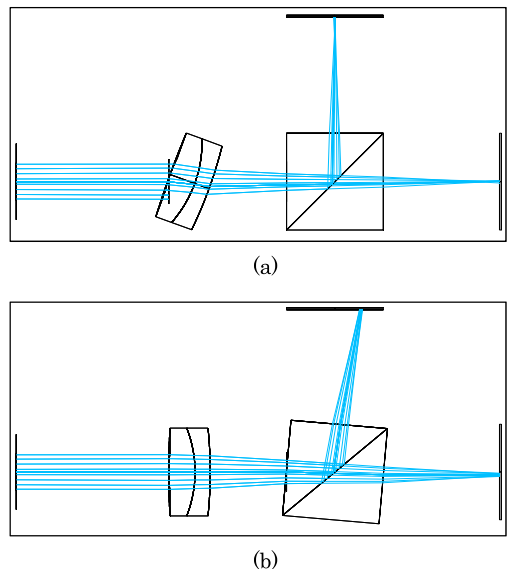


Fig. 7. Misalignments: (a) tilt of the cylindrical lens and (b) tilt of the beamsplitter.

focusing beams asymmetrical, and tilt along the Z axis changes the direction of the measuring beam. In this case, no fringes generate due to still having the same optical path of two arms of the interferometer. However, tilts of the beamsplitter will lead to a tilt of the optical axis, and thus the light beam will no longer travel on the same path, in which case straight fringes with equal intervals are generated on the image plane [Fig. 8(b)]. The simulated

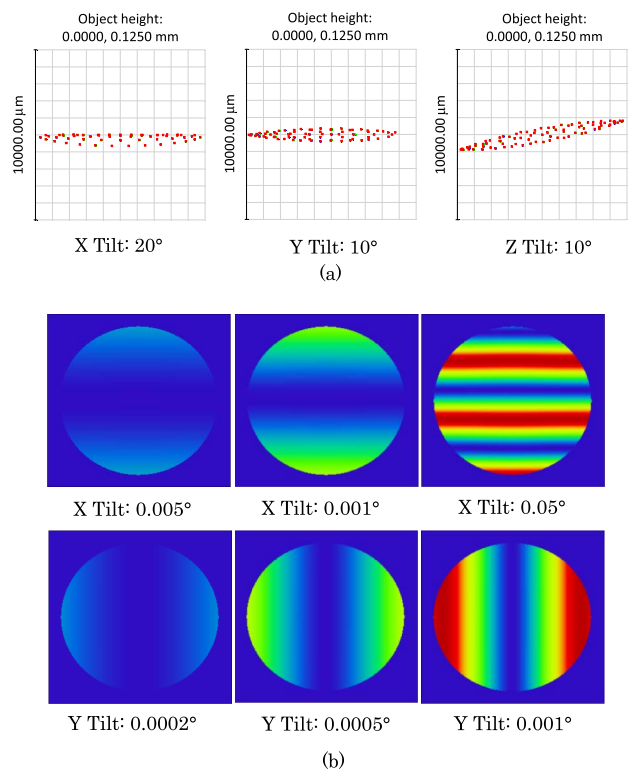


Fig. 8. Simulated results regarding tilts: (a) spot diagram and (b) interferograms.

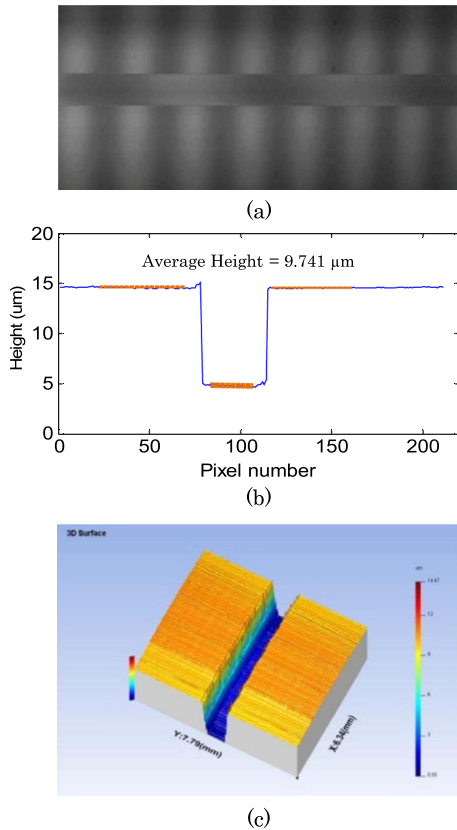


Fig. 9. Measurement result of a 9.759 μm step height sample: (a) captured interferogram, (b) 2D profile result, and (c) 3D surface map.

interferograms show that the OPD is very sensitive to tilts of the beamsplitter. This means more attention should be paid to the beamsplitter cube when carrying out alignments.

4. Results and Discussion

Two step height samples, respectively, made by Wyko and Rubert & Co. Ltd. were measured with this SD-LCI setup. The standard sample from Wyko has a single step calibrated with a height of 9.759 μm . The step sample from Rubert was manufactured with four steps (namely 30, 200, 500, and 1000 μm), and one of them with height of 30 μm was measured. Figures 9(a) and 10(a) show the captured interferograms when performing measurements of step surfaces, and Figs. 9(b) and 10(b) depict the corresponding profile results analyzed by the FFT algorithm. Supposing the heights given by the manufacturers were truth value, the relative errors of measurement can be calculated as follows:

$$e_r = \frac{|h_m - h_t|}{h_t} \times 100\%, \quad (11)$$

where h_t is the true value, h_m denotes the measured value, and e_r is the relative error.

At this experimental stage, these small relative errors of measurement depicted in Table 1 verify that

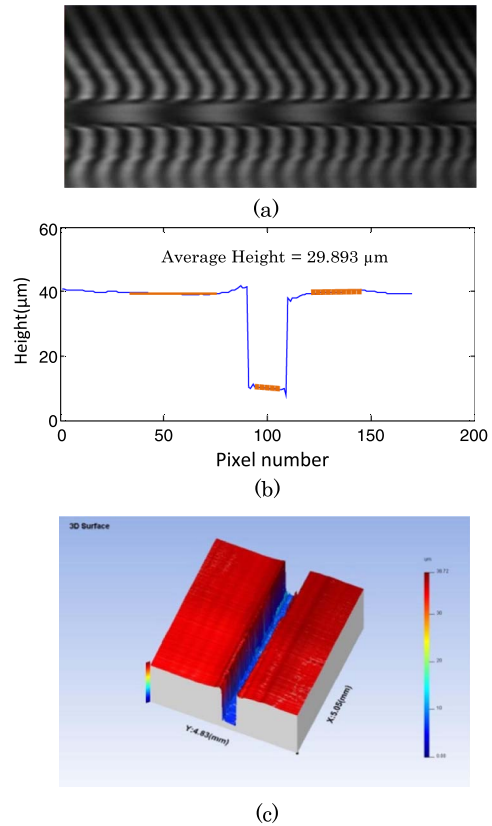


Fig. 10. Measurement result of a 30 μm step height sample: (a) captured interferogram, (b) 2D profile result, and (c) 3D surface map.

the profile results closely align with the parameters calibrated by the manufacturers and are reliable enough to be used for long profile measurement.

By translating the tested sample at a speed of 0.5 mm/s, on-line surface measurement was simulated as well. Figures 9(c) and 10(c), respectively, show 3D surface maps of the 9.759 μm step and the 30 μm step, which were constructed by more than 800 sampling profiles along the translating direction. Compared to current white light interferometers, this cylindrical-based SD-LCI shows considerable advantages when applied for fast and large-scale surface inspection.

Furthermore, the commercial instrument (Taly-surf CCI) was used to measure the same steps for the purpose of roughly providing our setup with the measurement references. The mean values of step height from Wyko are, respectively, 9.792 and 9.785 μm , corresponding to CCI and the proposed SD-LCI, and 29.964 and 29.859 μm for the 30 μm step height. Those close 3D results demonstrate again

Table 1. Relative Errors of Measurement

Height Values (μm)	Wyko	Samples Rubert
h_t	9.759	30
h_m	9.741	29.975
Relative errors e_r	0.18%	0.36%

that the proposed SD-LCI could be applied to a production line like the R2R surface inspection, where only defects on the film surface are concerned in terms of quality control.

5. Conclusions

A cylindrical lens-based spectral domain low-coherence interferometric technique for long profile on-line surface inspection is proposed. Obtaining a surface profile in a single shot allows this setup to minimize the effect of external perturbations and environmental noise when carrying out real-time measurement. With the aid of Zemax software, the alignment errors were analyzed, and it turns out that special attention should be paid to the misalignments of the beamsplitter used for generating the measurement arm and reference arm of the interferometer.

Finally, the performance of the SD-LCI was evaluated experimentally by measuring two step heights. The 2D profile results and 3D surface maps closely align with the calibrated specifications given by the manufacturer, as well as the measurement results by the other commercial instrument, which confirms that cylindrical-based SD-LCI could be applied to on-line surface inspection.

The authors gratefully acknowledge the UK's Engineering and Physical Sciences Research Council (EPSRC) funding of the First Grant (Grant Ref: EP/K007068/1), the funding of the EPSRC Centre for Innovative Manufacturing in Advanced Metrology (Grant Ref: EP/I033424/1), and the funding with Grant Ref: EP/K018345/1.

References

1. L. De Chiffre, H. Kunzmann, G. Peggs, and D. Lucca, "Surfaces in precision engineering, microengineering and nanotechnology," *CIRP Ann.* **52**, 561–577 (2003).
2. R. Maboudian, "Surface processes in MEMS technology," *Surf. Sci. Rep.* **30**, 207–269 (1998).
3. B. Bowe and V. Toal, "White light interferometric surface profiler," *Opt. Eng.* **37**, 1796–1799 (1998).
4. T. Li, A. Wang, K. Murphy, and R. Claus, "White-light scanning fiber Michelson interferometer for absolute position-distance measurement," *Opt. Lett.* **20**, 785–787 (1995).
5. P. Zhu and K. Wang, "Single-shot two-dimensional surface measurement based on spectrally resolved white-light interferometry," *Appl. Opt.* **51**, 4971–4975 (2012).
6. C. C. Scott, A. Lutttge, and K. A. Athanasiou, "Development and validation of vertical scanning interferometry as a novel method for acquiring chondrocyte geometry," *J. Biomed. Mater. Res. A* **72**, 83–90 (2005).
7. F. Gao, H. Muhamedsalih, and X. Jiang, "Surface and thickness measurement of a transparent film using wavelength scanning interferometry," *Opt. Express* **20**, 21450–21456 (2012).
8. J. K. Schmit, K. Creath, and J. Wyant, "Surface profilers, multiple wavelength, and white light interferometry," in *Optical Shop Testing*, 3rd ed. (Wiley, 2007), pp. 667–755.
9. M. Hart, D. G. Vass, and M. L. Begbie, "Fast surface profiling by spectral analysis of white-light interferograms with Fourier transform spectroscopy," *Appl. Opt.* **37**, 1764–1769 (1998).
10. P. Hlubina, "Dispersive white-light spectral interferometry to measure distances and displacements," *Appl. Opt.* **212**, 65–70 (2002).
11. K.-N. Joo and S.-W. Kim, "Absolute distance measurement by dispersive interferometry using a femtosecond pulse laser," *Opt. Express* **14**, 5954–5960 (2006).
12. D. S. Mehta, S. Saito, H. Hinosugi, M. Takeda, and T. Kurokawa, "Spectral interference Mirau microscope with an acousto-optic tunable filter for three-dimensional surface profilometry," *Appl. Opt.* **42**, 1296–1305 (2003).
13. X. Jiang, K. Wang, F. Gao, and H. Muhamedsalih, "Fast surface measurement using wavelength scanning interferometry with compensation of environmental noise," *Appl. Opt.* **49**, 2903–2909 (2010).
14. J. Schwider and L. Zhou, "Dispersive interferometric profilometer," *Opt. Lett.* **19**, 995–997 (1994).
15. J. Calatroni, C. Sáinz, and R. Escalona, "The stationary phase in spectrally resolved white-light interferometry as a refractometry tool," *J. Opt. Pure Appl. Opt.* **5**, S207–S210 (2003).
16. Y.-S. Ghim and S.-W. Kim, "Spectrally resolved white-light interferometry for 3D inspection of a thin-film layer structure," *Appl. Opt.* **48**, 799–803 (2009).
17. S. K. Debnath and M. P. Kothiyal, "Improved optical profiling using the spectral phase in spectrally resolved white-light interferometry," *Appl. Opt.* **45**, 6965–6972 (2006).
18. S. K. Debnath and M. P. Kothiyal, "Optical profiler based on spectrally resolved white light interferometry," *Opt. Eng.* **44**, 013606 (2005).
19. M. Takeda, H. Ina, and S. Kobayashi, "Fourier-transform method of fringe-pattern analysis for computer-based topography and interferometry," *J. Opt. Soc. Am.* **72**, 156–160 (1982).
20. C. Sainz, J. Calatroni, and G. Tribillon, "Refractometry of liquid samples with spectrally resolved white light interferometry," *Meas. Sci. Technol.* **1**, 356–361 (1990).
21. S. K. Debnath and M. P. Kothiyal, "Analysis of spectrally resolved white light interferometry by Hilbert transform method," *Proc. SPIE* **6292**, 62920P (2006).
22. S. K. Debnath, M. P. Kothiyal, and S.-W. Kim, "Evaluation of spectral phase in spectrally resolved white-light interferometry: comparative study of single-frame techniques," *Opt. Laser Technol.* **47**, 1125–1130 (2009).
23. H. Muhamedsalih, F. Gao, and X. Jiang, "Comparison study of algorithms and accuracy in the wavelength scanning interferometry," *Appl. Opt.* **51**, 8854–8862 (2012).